Check for updates

Steel Sheet Sheathed Cold-Formed Steel Framed In-line Wall Systems. II: Impact of Nonstructural Detailing

Amanpreet Singh, S.M.ASCE[1]; Xiang Wang[2]; Zhidong Zhang, S.M.ASCE[3]; Fani Derveni, S.M.ASCE[4]; Hernan Castaneda[5]; Kara D. Peterman, M.ASCE[6]; Benjamin W. Schafer, M.ASCE[7]; and Tara C. Hutchinson, M.ASCE[8]

Abstract: Although cold-formed steel (CFS) framing systems have the potential to support the need for resilient housing, the use of CFS has been restricted due to gaps in understanding its structural behavior and by the limited guidelines provided in design standards. In particular, the contribution from nondesignated lateral systems and portions of the building system not specifically designated by the design engineers has not been substantially investigated through experiments. To address these shortcomings, a two-phased experimental effort was undertaken to assess the impact of gravity walls, finish application, window openings, and their relationship with the designated lateral force–resisting system. The wall-line assemblies tested, which have shear walls placed in-line with gravity walls, adopted chord stud packs with a tie-rod assembly and were either unfinished or finished, and laid out in a symmetrical or unsymmetrical fashion. In addition, both Type I and Type II shear wall and anchorage detailing were investigated. In this paper, the impact of test variables governing the nonstructural detailing of CFS-framed walls has been quantified, and a companion paper presents findings regarding the impact of structural detailing. **DOI: 10.1061/(ASCE)ST.1943-541X.0003434.** *© 2022 American Society of Civil Engineers.*

Downloaded from ascelibrary.org by University of California, San Diego on 09/25/22. Copyright ASCE. For personal use only; all rights reserved.

Introduction

The North American construction industry, seeing an increasing need for low cost, multihazard-resilient buildings, has promoted the use of cold-formed steel (CFS) framing for midrise buildings (3-6 stories) in the recent years. CFS framing leads to lightweight structures with high durability and ductility, low installation costs, particularly when prefabricated assemblies are used, and low maintenance costs due to its resistance to corrosion (Schafer 2011). A high strength to weight ratio and an inherent noncombustible nature in addition to significant cost benefits has made CFS framing a popular choice for construction of low-rise and midrise structures. Although CFS framing systems have the potential to support the need for resilient housing, their use has been restricted due to gaps in understanding their structural behavior and consequentially the limited guidelines provided in design standards. There is limited understanding regarding the seismic response of complete systems for most construction types, however, particularly when nondesignated lateral systems and building systems not specifically designated by the design engineers have to be included. This issue is more significant when cold-formed steel wall braced components serve as the designated lateral force–resisting system of choice because they must be finished and laid out in conjunction with the architectural needs of the overall building. For example, walls often have openings (doors and windows) and have finishes installed (exterior and interior) for insulation purposes. In addition, the location of shear walls in a long wall line are often not symmetrically placed.

The need to understand the combination of structural and nonstructural finish materials for lightweight framing has been addressed to some extent for wood-framed shear walls. However, limited investigations of their impact on CFS-framed shear walls have been undertaken. For example, Uang and Gatto (2003) examined the effects of gypsum wallboard and stucco finish materials on the lateral behavior of wood-framed shear walls with oriented strand board (OSB) or plywood as sheathing. They concluded that finish materials have a substantial effect on the shear wall performance. Usually ignored in design applications, the nonstructural finish application increased the wall strength. To evaluate at a system level, Filiatrault et al. (2002) tested a 2-story wood-framed house structure with and without interior (gypsum board) and exterior (stucco) wall finish. Application of finish materials again led to an increase in lateral strength and stiffness of the wood-framed structure, accompanied with a decrease in deformation capacity. In concurrence with prior test program findings, these effects on performance were deemed significant and recommended to

[1]Ph.D. Candidate, Dept. of Structural Engineering, Univ. of California, San Diego, La Jolla, CA 92093. ORCID: https://orcid.org/0000-0001-8837-2105

[2]Associate Professor, School of Civil Engineering, Sun Yat-Sen Univ., Guangzhou 510275, China; formerly, Dept. of Structural Engineering, Univ. of California, San Diego, La Jolla, CA 92093.

[3]Ph.D. Candidate, Dept. of Civil and Systems Engineering, Johns Hopkins Univ., Baltimore, MD 21218. ORCID: https://orcid.org/0000-0002-4844-7907

[4]Postdoctoral Associate, Institute of Mechanical Engineering, École Polytechnique Fédérale de Lausanne, 1015 Lausanne, Switzerland; formerly, Dept. of Civil and Environmental Engineering, Univ. of Massachusetts, Amherst, MA 01003.

[5]Ph.D. Candidate, Dept. of Civil and Environmental Engineering, Univ. of Massachusetts, Amherst, MA 01003.

[6]Assistant Professor, Dept. of Civil and Environmental Engineering, Univ. of Massachusetts, Amherst, MA 01003.

[7]Professor, Dept. of Civil and Systems Engineering, Johns Hopkins Univ., Baltimore, MD 21218.

[8]Professor, Dept. of Structural Engineering, Univ. of California, San Diego, La Jolla, CA 92093 (corresponding author). ORCID: https://orcid.org/0000-0001-9109-7896. Email: tara@ucsd.edu

Note. This manuscript was submitted on September 2, 2021; approved on April 18, 2022; published online on September 22, 2022. Discussion period open until February 22, 2023; separate discussions must be submitted for individual papers. This paper is part of the ***Journal of Structural Engineering***, © ASCE, ISSN 0733-9445.

be considered in design. Based on several such component and system level tests, ASCE/SEI (2017) Table 12-1 provides the expected strength values for different types of finishes for wood-framed shear walls. In contrast, no such summarized strength data exist for CFS-framed walls to aid the designer when such walls are finished.

For CFS-framed walls, several studies have examined the impact of gypsum panel sheathing on the walls' lateral resistance (e.g., Nguyen et al. 1996; Morgan et al. 2002; Morello 2009; Liu et al. 2014; Lu 2015). For example, Liu et al. (2014) reported that using gypsum panels on the interior face of OSB sheathed CFS shear walls increased the wall initial stiffness and may also slightly increase wall strength. On a structural system level, one phase of the building specimen test program within the CFS-NEES program included nonstructural components such as exterior sheathing of the perimeter gravity walls, gypsum-board sheathing of the interior of the perimeter gravity and OSB sheathed shear walls, interior partition walls, ceilings, staircases, and exterior weatherproofing (Peterman et al. 2016). These tests demonstrated that the nonstructural systems significantly altered the dynamic characteristics of the building, while also increasing the lateral load capacity of the building. The fundamental period decreased from 0.32 and 0.36 s to 0.15 and 0.26 s in the long and short directions of the building, respectively.

Compared with other available sheathing options, the use of steel sheets as sheathing is relatively new. Research conducted by Yu et al. (2007), Yu (2010), Ong-Tone (2009), Shamim et al. (2013), Balh et al. (2014), DaBreo et al. (2014), and several others have contributed to the development of the current North American standards, American Iron and Steel Institute (AISI) S240 (AISI 2015a) and AISI S400 (AISI 2015b), providing a basis for designing shear walls with steel sheet sheathing. However, the impact of finishes on the lateral resistance of shear walls with steel sheet sheathing has not been adequately explored. As a result, definitive strength predictions for finish systems are not widely available; thus, the current design codes do not take into account the effect of finish application on wall behavior.

Another nonstructural element whose impact on wall behavior has not been adequately considered in research is the presence of openings, such as windows and doors. Nonetheless, the design of Type I CFS-framed shear walls typically includes fully sheathed shear walls with tie-downs at each end. These walls are permitted to have openings provided details are incorporated to account for force transfer around openings. Previous studies have often considered openings as perforations in the sheathing and thus examined the decrease in wall lateral strength. For example, Steel Framing Alliance (1997) tested 12-m long shear walls with varying opening areas, and observed that walls with larger sheathing areas demonstrated greater strengths. Similarly, Salenikovich et al. (2000) compared the performance of 12-m long CFS-framed walls with and without openings, considering openings as perforations in the designated lateral force–resisting system. Despite these and other prior studies on single walls with window openings, their impact as a nonstructural component in-line with multiple shear walls has not been systematically evaluated.

The experimental program discussed herein was designed to include test variables that address the aforementioned limitations in an effort to enrich the experimental database documenting the performance of steel sheet sheathed CFS-framed wall assemblies. Specifically, in this paper, the impact of test variables governing the nonstructural detailing of CFS-framed walls is discussed. Nonstructural detailing of interest include finish application, window opening, and unsymmetrical shear wall layout. Wall behavior in this program is quantified through a series of full-scale dynamic and quasi-static tests. In a companion paper, the impact of structural detailing, namely, tie-down and anchorage systems, on several wall performance metrics are of focus (Singh et al. 2022b). Details regarding the experimental program, test matrix, wall detailing, test setup, test protocol, and instrumentation are also provided in the companion paper. For brevity, details relevant to the nonstructural variables considered are reproduced in the following section.

Experimental Program

The wall-line test program within the project, coined as the CFS-NHERI project, was a two-phased experimental program. The first phase of the experimental program involved testing pairs of wall-line assemblies, shear walls placed in-line with gravity walls, at the NHERI Large High-Performance Outdoor Shake Table (LHPOST) at the University of California, San Diego (Van Den Einde et al. 2004). Two nominally identical walls each for eight unique wall configurations, amounting to 16 walls in total, were tested during this shake-table test phase. The second phase of the experimental program involved testing single wall-line configurations under quasi-static cyclic displacement controlled loading conditions using hydraulic actuators at the University of California, San Diego, Structural Engineering Powell Laboratory. This phase of testing involved 10 wall configurations, including two configurations common with the eight configurations tested at the shake table. In total, 16 unique wall configurations were tested between the two test phases. Table 1 details the wall configurations tested during the two phases of the test program, and additional details have been given by Singh et al. (2022b).

The test matrices include specimens with varying configurations of shear and gravity segments in-line with each other. Shear wall segments were detailed with tie-down assemblies consisting of compression stud packs and tension tie-rods with a steel sheet sheathing on single side. The various configurations in the test matrix included specimens in an unfinished or finished, symmetrical or unsymmetrical, Type I or Type II shear wall detailing configuration, tie-rods or hold-downs as anchorage detailing, and with or without a window opening. Tested wall specimens were 4.88-m (16-ft) long and 2.74-m (9-ft) high. The wall details were motivated by a CFS-framed archetype building designed according to current code guidelines and recently available experimental data (Singh et al. 2020a). Selected details reflect the shear and gravity detailing from approximately the midheight floors within the 10-story building or bottom floor of a 4-story building. Compression stud packs with tension tie-rods, a common detail seen in multi-story building design, provide wall overturning and uplift restraint.

Specimen names refer to the characteristics of each 1.22-m (4-ft) quadrant length of the 4.88-m (16-ft) specimen appended with a number indicating whether it was a Type I or Type II wall system as defined by AISI S400 (AISI 2015b), specifying the locations of tension tie-rods. For example, SWWS-2 is a Type II *Shear-Window-Window-Shear* wall-line specimen with tension tie-rods located at wall-line end [Fig. 1(a)]. During the quasi-static cyclic test phase, two concrete slabs were used to apply a total of 12.4 kN/m (850 lb/ft) gravity load. Two hydraulic 220-kN actuators with ±60-cm stroke, used in parallel (total lateral load capacity of 440-kN), were employed to push and pull along the wall longitudinal axis. The walls were subjected to a displacement controlled cyclic Consortium of Universities for Research in Earthquake Engineering (CUREE) protocol (Krawinkler et al. 2001). The specimens were reverse cyclically tested until a 60% postpeak strength degradation was observed.

A similar combination of concrete slabs with steel trench plates was employed to apply a seismic weight of 14.6 kN/m (1,000 lb/ft)

Downloaded from ascelibrary.org by University of California, San Diego on 09/25/22. Copyright ASCE. For personal use only; all rights reserved.

Table 1. Test matrix and definition of specimens

Test phase	Specimen	Description	Tie-down detailing	Shear wall detailing	Finish	
					Exterior face	Interior face
Shake table test phase (two each)	SGGS-1	Baseline specimen. Symmetrical shear segments on both wall ends	Tension tie-rods	Type I	—	—
	SGGS-1XS	SGGS-1 with finer steel sheet fastener pattern	Tension tie-rods	Type I	—	—
	SGGS-1F	SGGS-1 with finish	Tension tie-rods	Type I	EIFS	Gypsum
	SGGS-1SB	SGGS-1 with composite steel sheet glass-mat panels	Tension tie-rods	Type I	EIFS	Gypsum
	SGGS-2B	SGGS-2 with coarser steel sheet fastener pattern	Tension tie-rods	Type II	—	—
	SGGG-1	Unsymmetrical wall: shear segment on one wall end only	Tension tie-rods	Type I	—	—
	SWWS-1	SGGS-1 with window opening in the middle bays	Tension tie-rods	Type I	—	—
	SWWS-2	SGGS-2 with window opening in the middle bays	Tension tie-rods	Type II	—	—
Quasi-static test phase (one each)	SGGS-2	Symmetrical: shear segments on both wall ends	Tension tie-rods	Type II	—	—
	SGGS-2F	SGGS-2 with finish	Tie-rods	Type II	EIFS	Gypsum
	SWWS-1	SGGS-1 with window opening in the middle bays	Tension tie-rods	Type I	—	—
	SWWS-2	SGGS-2 with window opening in the middle bays	Tension tie-rods	Type II	—	—
	SWWS-2F	SWWS-2 with finish	Tension tie-rods	Type II	EIFS	Gypsum
	SGGG-1F	SGGG-1 with finish	Tension tie-rods	Type I	EIFS	Gypsum
	SGGS-1HD	SGGS-1 with hold-downs	Hold-downs	Type I	—	—
	SGGS-1HDF	SGGS-1HD with finish	Hold-downs	Type I	EIFS	Gypsum
	GGGG	Gravity frames in all bays	None	N/A	—	Gypsum
	GGGG-F	GGGG with exterior finish	None	N/A	EIFS	Gypsum

Source: Reprinted from Singh et al. (2022b).
Note: Specimen names indicate characteristics of each quadrant length appended with a number for shear wall detailing and additional characters for differences in finish, fastener detail, and tie-down detail. EIFS = exterior insulation finishing system.

Fig. 1. (a) Specimen SWWS-2 as installed in test setup; (b) jamb stud built-up section used around window opening; (c) front view of exterior face of Specimen SGGS-2F; and (d) isometric view of interior face of Specimen SGGS-2F.

Downloaded from ascelibrary.org by University of California, San Diego on 09/25/22. Copyright ASCE. For personal use only; all rights reserved.

per wall during the shake table tests phase. These wall specimens were tested under a sequence of increasing intensity earthquake motions applied in the east–west direction using the single-axis shake table, which aligned with the longitudinal axis of the wall specimens. Select wall pair specimens were tested under slow monotonic pull conditions until a 40% postpeak strength degradation was observed. Due to this, wall strength data in the negative direction are not available for these wall specimens. The slow monotonic pull tests were performed by slowly moving the shake table platen, and the top of the wall pairs was connected to a reaction frame. However, during quasi-static cyclic tests, use of hydraulic actuators allowed for an extended postpeak behavior evaluation. Between earthquake tests, low-amplitude white-noise tests were conducted before and after to determine the dynamic characteristics of the wall specimens at different damage stages.

Application of Finish Materials

Finish application for the wall configurations in the two test matrices was performed after installing the wall specimens into the test setup (specimens with finish application in Table 1). Gypsum boards on the interior face and glass-mat sheathing panels on the exterior face were installed while the specimens were erected in their test setups using No. 8 gauge 44-mm (1.75-in.) flat-head screws at 152-mm (6-in.) on center (o.c.) edge and 406-mm (16-in.) o.c. field spacing [Fig. 2(a)]. Installed gypsum boards were 1.22-m (4-ft) × 2.44-m (8-ft) × 16-mm (5/8-in.) Firecode Type X, and the glass-mat sheathing panels were 1.22-m (4-ft) × 2.74-m (9-ft) × 16-mm (5/8-in.) Firecode Type X.

On top of the glass-mat sheathing panels on the exterior face, first, 25-mm (1-in.)-thick expanded polystyrene (EPS) foam boards were attached using cement adhesive. The foam boards were rasped down before applying a base coat, [Fig. 2(b)]. Subsequently, a reinforcing mesh was embedded into the base coat during its application, and a second coat was applied over the mesh base coat before applying a final finish coat as the last step [Fig. 2(c)]. The different layers of the exterior insulation finish system (EIFS) were applied over a period of 3 days. The selection of these finish details were based on discussions with practicing engineers, with EIFS being one of the most common exterior finish choices. Use of gypsum panels on the interior face was motivated by their widespread application in corridors for fire protection.

Detailing around Window Opening

To support the force transfer around window openings, the jamb studs, sill and header tracks were sized per design codes AISI S240 (AISI 2015a) and AISI S100 (AISI 2016). A window opening

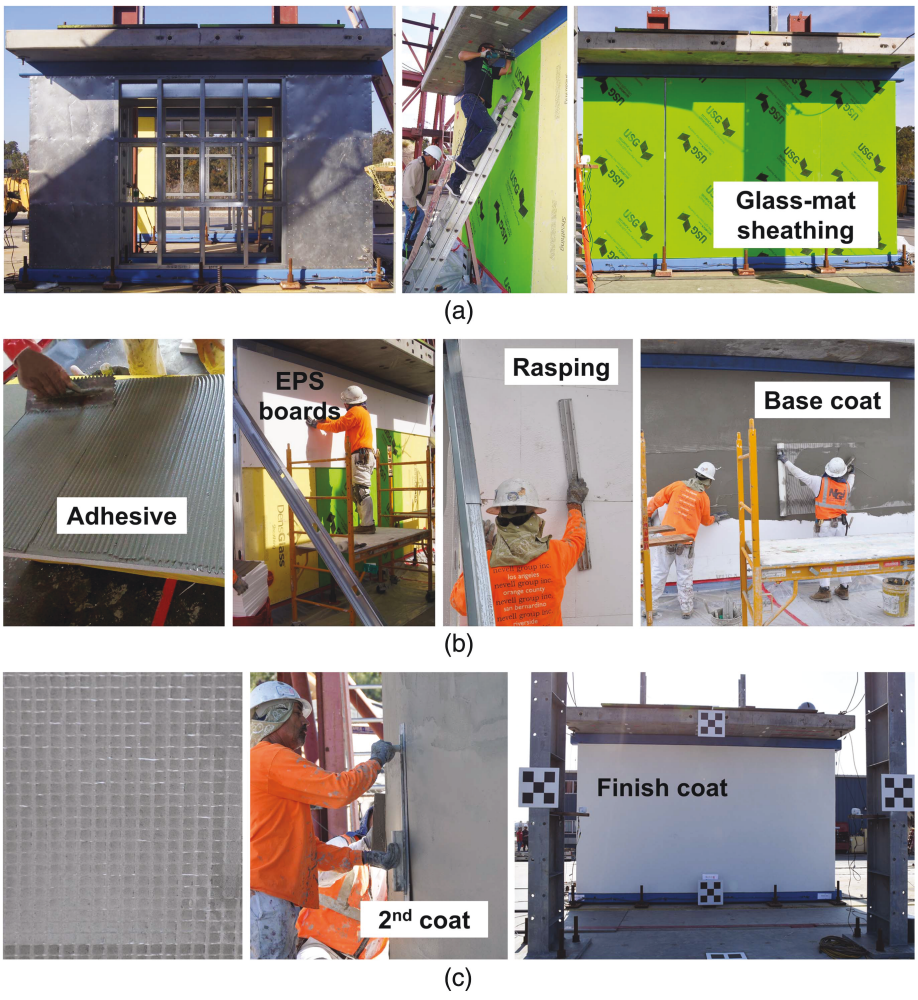

Fig. 2. Steps involved in exterior face finish application: (a) installation of glass-mat sheathing panels; (b) application of EPS foam boards using adhesive onto panel substrate followed by rasping of foam boards and application of base coat; and (c) embedded reinforcing mesh in base coat and application of second layer and finish coat.

J. Struct. Eng., 2022, 148(12): 04022194

Downloaded from ascelibrary.org by University of California, San Diego on 09/25/22. Copyright ASCE. For personal use only; all rights reserved.

2.18-m (7-ft 2-in.) wide and 1.22-m (4-ft) tall with a sill height 0.76-m (2-ft 6-in.) was installed within the middle 2.44-m (8-ft) bay. This opening would occupy the same space as the gravity bay in the baseline specimen, and hence would similarly have one 1.22-m (4-ft) shear wall segment at each end. Jamb studs were built-up members that utilized 600S250-68 stud and 600T250-97 track members as shown in Figs. 1(a and b). Similarly, the header track was also a built-up member using the same framing members, and the sill track used a single 600T250-97 track member, and the cripple region utilized 600S250-68 studs. Similar components were used for the fabrication of all other wall specimens. Both Type I (SWWS-1) and Type II (SWWS-2) wall-line assemblies with window openings were considered in the test program. One specimen with both a window opening and finish application, SWWS-2F, was also included in the test matrix.

Results and Discussion

In this section, the impact of test configuration variables pertaining to the nonstructural detailing is discussed by comparing select groups of specimens systematically. In like fashion, in the companion paper (Singh et al. 2022b), the impact of structural detailing variables on the CFS wall-line performance is discussed. The findings are presented in terms of key measured parameters and observed physical evidence.

Effect of Finish Application

Five pairs of finished-unfinished wall configurations were identified amongst the suite of specimens tested. Figs. 3(a and c) show the force-displacement response comparison of two such pairs, namely SGGS-1 with SGGS-1F and SGGS-2 with SGGS-2F. The Type I specimen pair was tested at the shake table, whereas the Type II specimen pair was tested within the quasi-static test setup. Nonetheless, the impact of loading history was not pronounced because it can be seen that the finish application consistently increased the lateral capacity of the specimen, V_u, without significant changes in the drift at which strength is achieved, Δ_{Vu}.

Elastic stiffness, K, defined as the secant stiffness at 40% strength, was also consistently increased due to finish application. Specifically for specimens tested within the shake table test phase, for the finished Specimen SGGS-1F, the accumulation of damage through the earthquake test sequence led to an elongation of the fundamental period from 0.082 s in its undamaged state to 0.201 s following the design-level earthquake test, compared with the unfinished Specimen SGGS-1, for which period elongation ranged from 0.157 to 0.199 s. Similarly, the damping ratio for SGGS-1F increased from 3.3% in its undamaged state to 7.9% after the design-level earthquake test compared with SGGS-1, for which the damping ratio changed from 2.1% to 5.3%.

Figs. 3(b and d) show backbone comparisons of the five pairs of unfinished and finished wall configurations, further corroborating

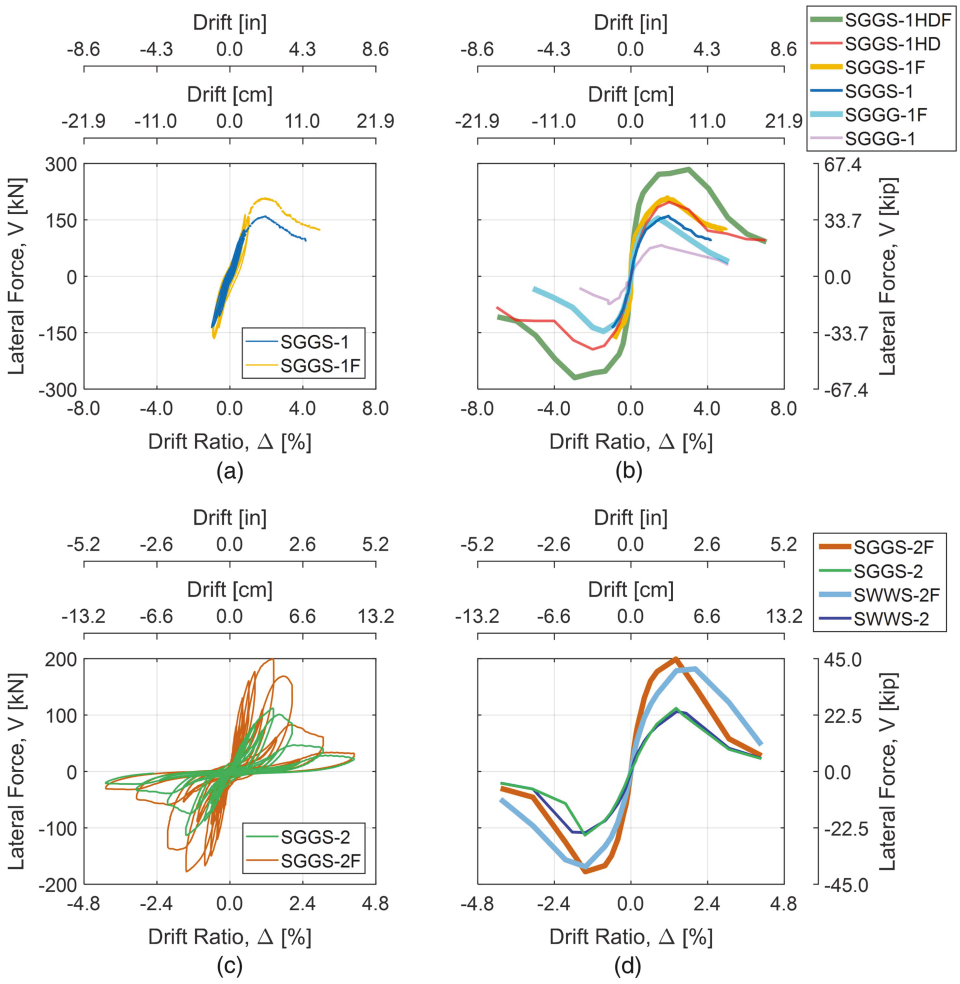

Fig. 3. Effect of finish application: (a) force-displacement response for Type I specimens; (b) backbone curve comparison for Type I specimens; (c) force-displacement response for Type II specimens; and (d) backbone curve comparison for Type II specimens.

J. Struct. Eng., 2022, 148(12): 04022194

Downloaded from ascelibrary.org by University of California, San Diego on 09/25/22. Copyright ASCE. For personal use only; all rights reserved.

Table 2. Effect of finish application: results summary

Test phase	Specimen	Wall strength, V_u (kN)	Drift ratio at $0.4V_u$ (prepeak), $\Delta_{0.4Vu}$ (%)	Drift ratio at V_u (peak), Δ_{Vu} (%)	Drift ratio at $0.8V_u$ (postpeak), $\Delta_{0.8Vu}$ (%)	Elastic stiffness,[a] K (kN/cm)
Shake table	SGGS-1	160.2	0.28	1.95	2.79	84.5
		—	−0.29	—	—	81.5
	SGGS-1F	208.2	0.15	1.90	3.14	205.9
		—	−0.13	—	—	237.1
	SGGG-1	82.7	0.32	1.60	2.76	37.1
		−72.3	−0.26	−1.08	−1.53	41.0
Quasi-static	SGGG-1F	156.8	0.17	1.41	2.35	74.7
		−144.5	−0.23	−1.43	−2.36	53.1
	SGGS-2	113.3	0.36	1.41	1.89	46.2
		−111.8	−0.37	−1.44	−1.68	44.4
	SGGS-2F	199.2	0.20	1.41	1.90	141.9
		−177.7	−0.21	−1.43	−1.85	121.7
	SWWS-2	107.2	0.30	1.43	2.13	52.6
		−107.3	−0.29	−1.43	−2.17	54.1
	SWWS-2F	181.8	0.29	2.01	2.66	91.9
		−169.0	0.29	−1.42	−2.41	84.7
	SGGS-1HD	197.4	0.35	1.99	3.36	82.9
		−194.3	−0.32	−2.00	−3.57	89.5
	SGGS-1HDF	284.7	0.17	3.01	4.13	237.3
		−269.2	−0.18	−2.94	−4.03	223.9

[a]When information about wall strength is not available in the negative direction, for stiffness calculations, the strength was assumed to be the same as the positive direction; 1 kN = 0.225 kip; and 1 kN/cm = 0.57 kip/in.

the aforementioned conclusions across all considered variables. Finally, a summary of key response measurements is provided in Table 2 with a visualization of these parameters provided in Fig. 4. Using a single additive strength model [Eq. (1)] and linear regression, it was measured that the finish application added 14.66 kN/m (1,005 lb/ft) to wall lateral strength

$$V_{u,\text{finished}} = V_{u,\text{unfinished}} + (\Delta v_{\text{EIFS}} + \Delta v_{\text{gypsum}}) \times L \quad (1)$$

where L = length of a wall; and $V_{u,\text{finished}}$ and $V_{u,\text{unfinished}}$ = wall lateral strengths for a finished and unfinished specimen, respectively.

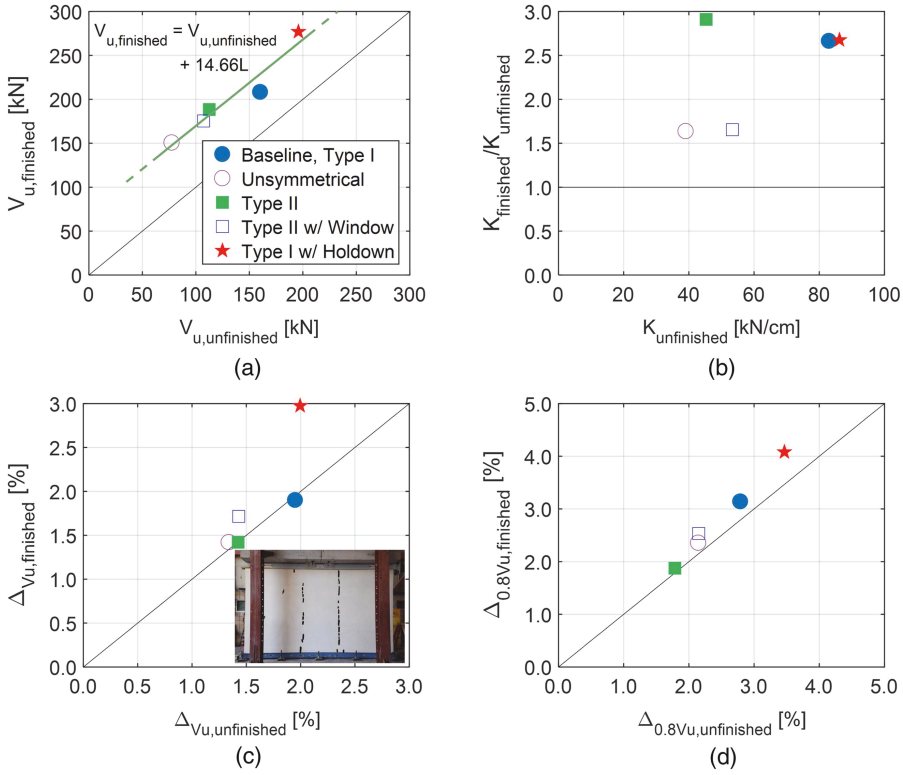

Fig. 4. Effect of finish application on key parameters: (a) lateral strength; (b) elastic stiffness; (c) drift at strength with Specimen SGGS-2F EIFS layer surface damage at strength; and (d) drift at 80% strength postpeak.

Downloaded from ascelibrary.org by University of California, San Diego on 09/25/22. Copyright ASCE. For personal use only; all rights reserved.

Assuming that 5.4 kN/m (370 lb/ft) was contributed by gypsum panels, Δv_{gypsum}, attached to CFS framing at a 150-mm perimeter spacing (Schafer et al. 2020), from the EIFS layer, the estimated increase in strength Δv_{EIFS} is calculated as 9.3 kN/m (635 lb/ft). The slope of the best-fit line from linear regression being close to unity indicates that the increase in lateral strength is independent of the underlying wall framing details. This is consistent with an additive strength model hypothesis. The elastic stiffness K was also 1.5–3 times higher for finished wall specimens compared with unfinished specimens [Fig. 4(b)]. Finally, in no case was the drift at strength, Δ_{Vu}, or the drift at 80% postpeak strength, $\Delta_{0.8Vu}$, negatively affected due to the application of finishes.

For finished specimens, damage observations during the test were limited to the damage in the EIFS layer and gypsum panels because the underlying framing members were not visible. Here, the damage observed in a finished Specimen SGGS-2F is described. Initially, hairline cracks in the EIFS layer began to appear at approximately 0.6% drift ratio. Minor crushing along gypsum panel edges and partial screw pull-through was also observed at this drift ratio. Appreciable visible separation of the EIFS layer from the CFS framing was observed at wall corners at 1.4% drift ratio. This was also accompanied by almost-full-height vertical surface cracks in the EIFS where the glass-mat sheathing panel edges existed [Fig. 4(c)]. The majority of the gypsum panel screws along the entire wall height also showed some degree of screw pull-through at this stage.

At about 2% drift ratio, separation at the wall ends of the EIFS from the framing was visible, particularly along the bottom, but detachment extended approximately half the wall height. By 3% drift ratio, the EIFS layer could be seen warped out-of-plane as the layer separation from steel sheet and framing propagated toward the middle from both wall ends. At this stage, gypsum panels had completely detached along one panel edge or fallen off. The EIFS layer had also almost entirely detached from the CFS framing as the drift demand increased to 5%. The detachment of finish layer allowed inspection for damage to any framing members. Notably, gravity studs adjacent to the shear wall segment compression stud packs had buckled locally. Select framing screws attaching the compression stud packs failed in shear at their head, resulting in the stud packs slipping and damaging the bottom track locally.

The damage to framing members observed in finished specimens is consistent with the damage observed in unfinished specimens. However, it is expected that the adherence of glass-mat panels to the steel sheet may have stabilized sheet buckling initially and delayed damage to fasteners. Even though the damage observations presented here are from a particular specimen, the progression of damage was similar for all finished specimens. Fig. 5 provides examples of the aforementioned damage observed in the finished Specimen SGGS-1F after removing it from the test setup following its attainment of a maximum drift ratio $\Delta_{\max}$ of 4.92%.

Fig. 6 shows the comparison of tension tie-rod force evolution between two finished and unfinished wall configuration pairs, namely the SGGS-2 and SGGS-2F pair and the SWWS-2 and SWWS-2F pair. Tie-rod forces are plotted against increases in lateral force (V/V_u) and lateral drift (Δ/Δ_{Vu}). For each measurement, response in only the direction of interest (push or pull) has been shown through indicated traces, and the response in the opposing direction is grayed out. For the same amount of normalized lateral drift, tension rods in finished specimens experienced larger axial forces when compared with unfinished specimens [Figs. 6(a and b)]. However, when normalized for individual specimen strengths, the difference in tension tie-rod force evolution is not as pronounced, even though finished specimens are nominally

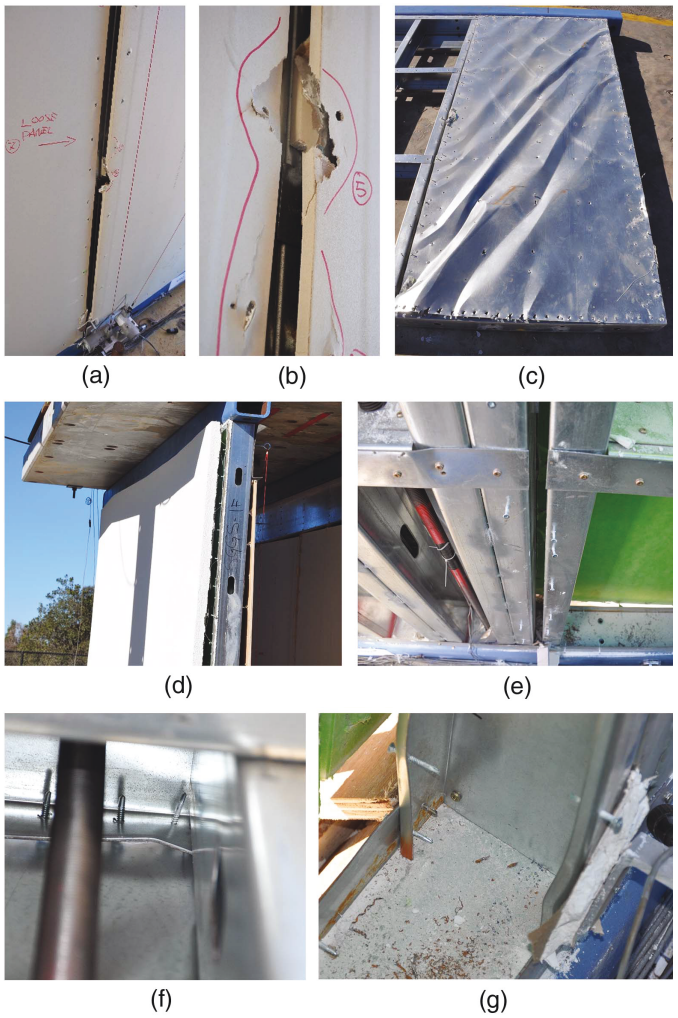

Fig. 5. (a–g) Physical damage to Specimen SGGS-1F following the testing sequence, $\Delta_{\max} = 4.92\%$ and $\Delta_{\text{res}} = 2.29\%$. The EIFS finish was manually removed to inspect the state of the steel sheathing, which articulated a well -defined plastic diagonal tension zone shown in plot (c).

subjected to larger axial forces [Figs. 6(c and d)]. Due to the larger stiffness of the finished specimens, SGGS-2F and SWWS-2F experienced greater lateral force compared with SGGS-2 and SWWS-2 for the same lateral drift, resulting in larger axial force carried by the tension tie-rods.

A comparison of wall end uplift evolution between finished and unfinished wall specimens with increasing normalized lateral force and drift is presented in Fig. 7. These analyses show that finished specimens experienced only slightly larger wall uplift at their ends when compared with unfinished counterparts. Although small, the increased wall end uplift at comparable normalized lateral load may explain variations in shear distortion among finished and unfinished pairs. Because the contribution toward drift due to uplift is larger for finished walls, the contribution of panel shear distortion toward drift, Δ^{γ}, is lower (Fig. 8).

Effect of Window Opening

Three unique wall configurations included a window opening in the middle 2.44-m bay rather than a gravity bay. This allowed for direct comparison between walls with and without openings, the later

Downloaded from ascelibrary.org by University of California, San Diego on 09/25/22. Copyright ASCE. For personal use only; all rights reserved.

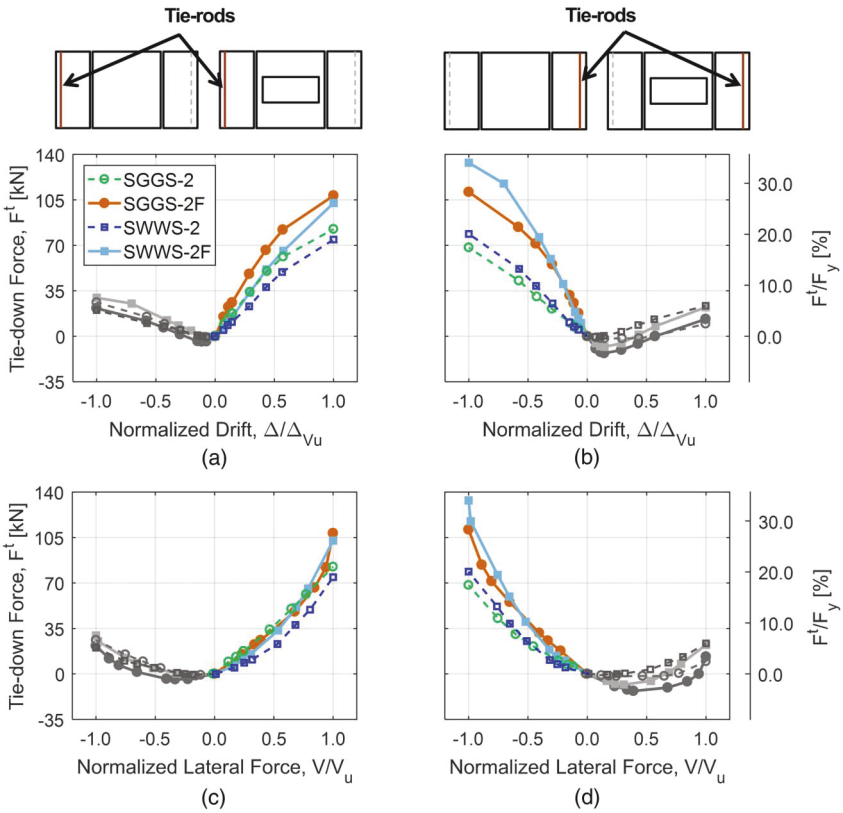

Fig. 6. Effect of finish on tension-rod forces with increase in (a and b) normalized drift; and (c and d) normalized lateral force.

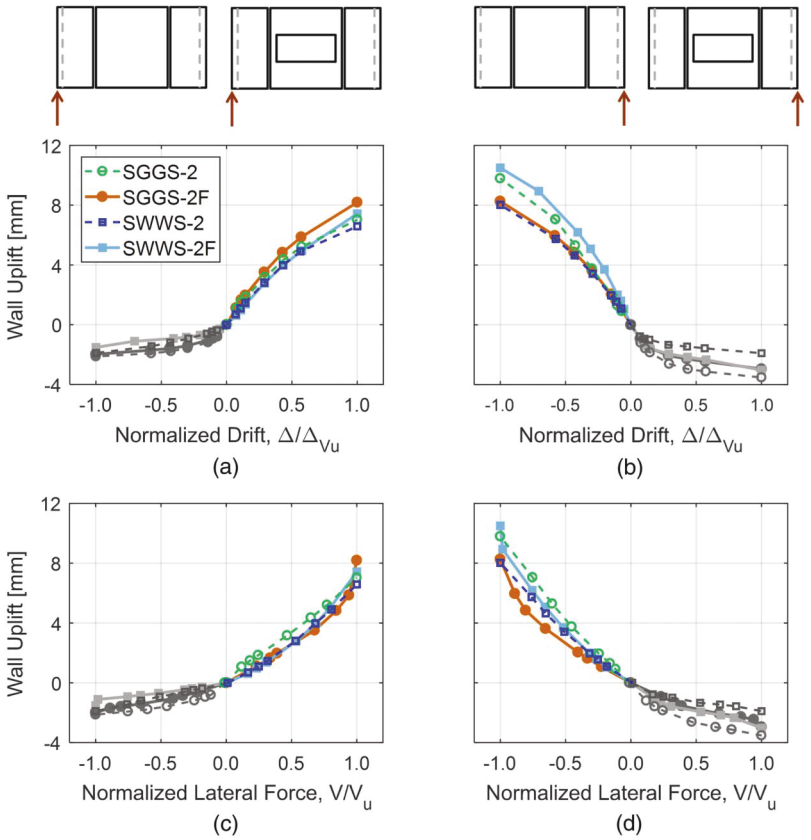

Fig. 7. Effect of finish on wall end uplift with increase in (a and b) normalized drift; and (c and d) normalized lateral force.

Downloaded from ascelibrary.org by University of California, San Diego on 09/25/22. Copyright ASCE. For personal use only; all rights reserved.

Downloaded from ascelibrary.org by University of California, San Diego on 09/25/22. Copyright ASCE. For personal use only; all rights reserved.

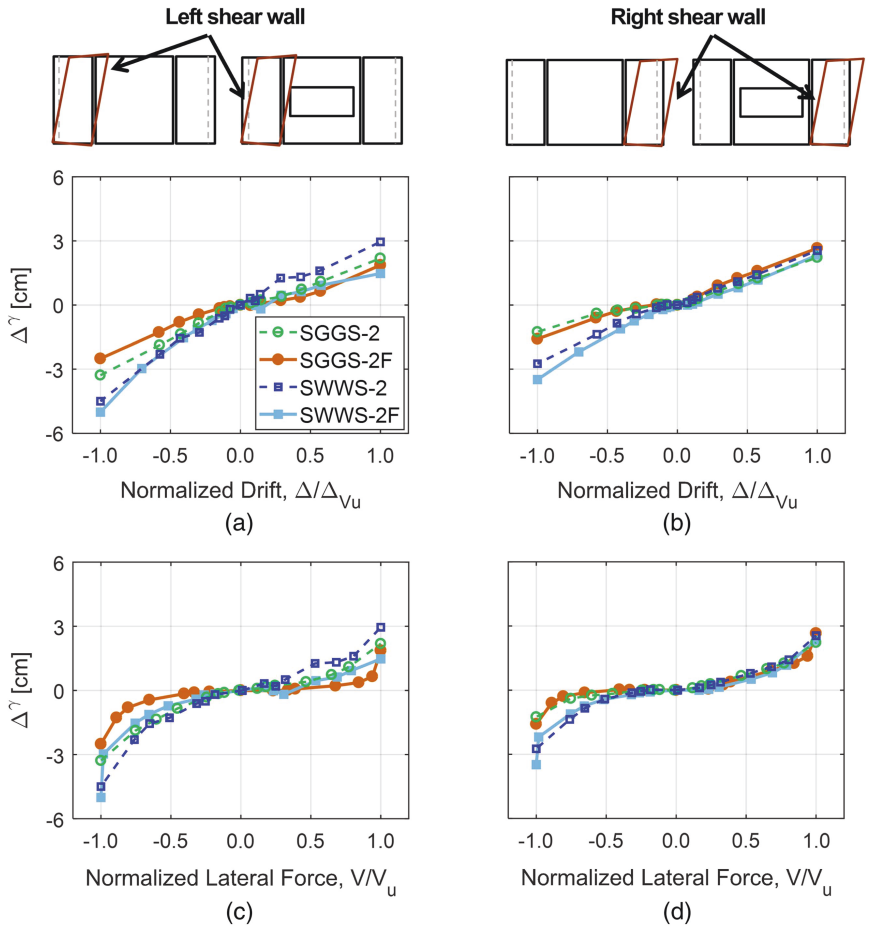

Fig. 8. Effect of finish on shear wall shear distortion with increase in (a and b) normalized drift; and (c and d) normalized lateral force.

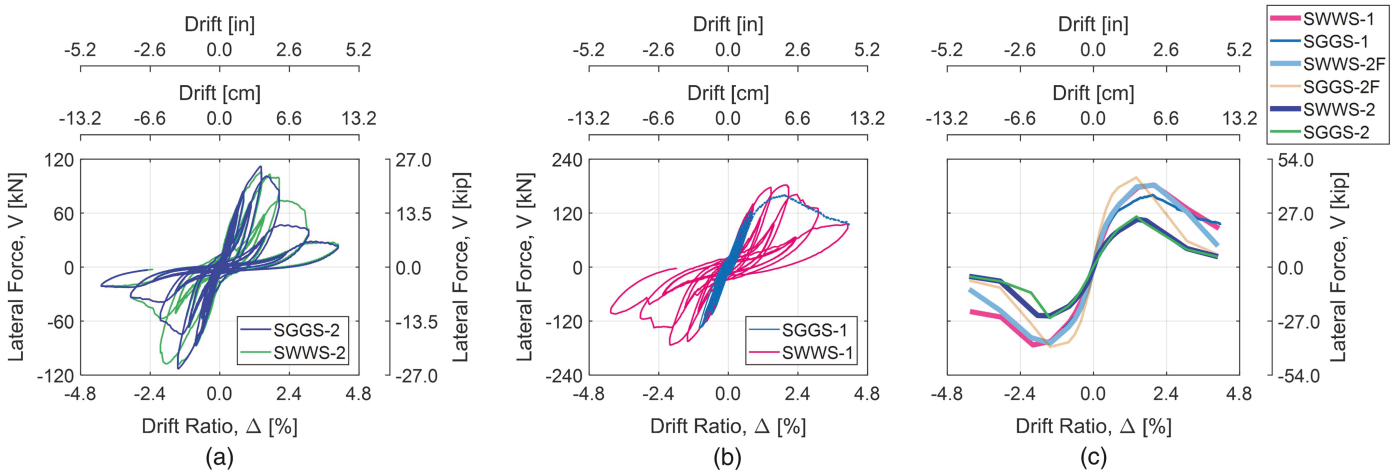

Fig. 9. Effect of window opening: force-displacement response for (a) Type II specimen pair; (b) Type I specimen pair; and (c) backbone curve comparison for Type I and Type II specimens.

referred to as a gravity bay. Fig. 9(a) shows a force-displacement response comparison between wall Specimens SGGS-2 and SWWS-2, and Table 3 summarizes key response measurements of the tested specimen pairs. From the figure, it can be seen that the presence of an opening did not have a significant impact on the global hysteresis response. Moreover, the lateral strengths for the two specimens were within 10% of each other. Additional specimen pairs shown in Fig. 9(c) comparing the backbones of varying window-no-window wall pairs consistently showed that the lateral strengths are within 10% of each other. In general, there was little to no impact on lateral strength, drift at strength, and elastic stiffness due to the presence of a window opening.

Damage to specimens with a wall opening developed initially with a well-defined tension field in the steel sheets. Yielding within

Table 3. Effect of window opening: results summary

Test phase	Specimen	Wall strength, V_u (kN)	Drift ratio at $0.4V_u$ (prepeak), $\Delta_{0.4Vu}$ (%)	Drift ratio at V_u (peak), Δ_{Vu} (%)	Drift ratio at $0.8V_u$ (postpeak), $\Delta_{0.8Vu}$ (%)	Elastic stiffness, K (kN/cm)
Shake table	SGGS-1	160.2	0.28	1.95	2.79	84.5
		—	−0.29	—	—	81.5
Quasi-static	SWWS-1	182.5	0.34	1.97	2.74	79.1
		−173.3	−0.36	−2.00	−2.58	70.4
	SGGS-2F	199.2	0.20	1.41	1.90	141.9
		−177.7	−0.21	−1.43	−1.85	121.7
	SWWS-2F	181.8	0.29	2.01	2.66	91.9
		−169.0	0.29	−1.42	−2.41	84.7
	SGGS-2	113.3	0.36	1.41	1.89	46.2
		−111.8	−0.37	−1.44	−1.68	44.4
	SWWS-2	107.2	0.30	1.43	2.13	52.6
		−107.3	−0.29	−1.43	−2.17	54.1

Note: 1 kN = 0.225 kip; and 1 kN/cm = 0.57 kip/in.

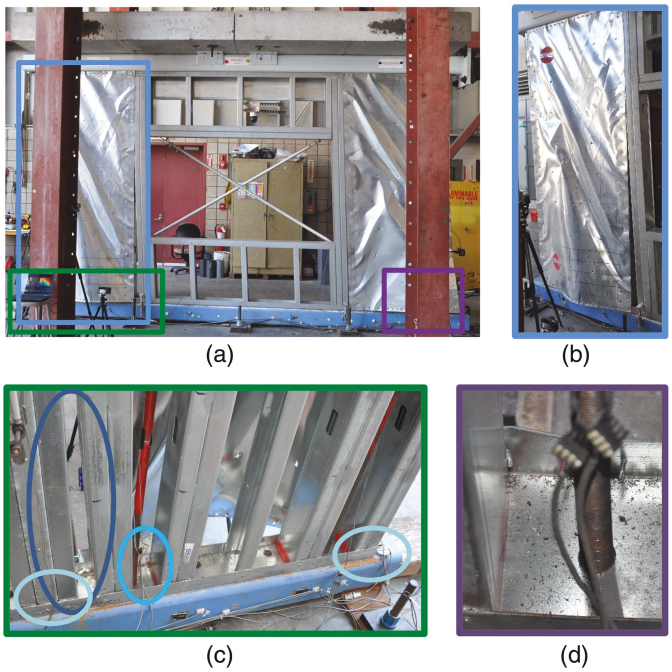

Fig. 10. (a–d) Physical damage to Specimen SWWS-1 at drift ratio $\Delta = +4.12\%$.

the steel sheet progressed with increasing drift demand similar to that manifested in specimens without a window opening. However, damage to framing members differed significantly for the two configurations. At approximately 1% drift ratio, a small gap became visible at the corners of the window as the rectangular opening deformed. Due to force transfer around the opening, compression stud packs adjacent to the opening experienced higher stresses. This resulted in an approximately 1-cm-wide gap developing between the stud packs and window jamb stud. These additional stresses led to failure in shear of the screws attaching the compression stud packs to the bottom track at 3% drift ratio. As drift demand increased, the now-detached stud packs slipped along the bottom track and began to bear against the tension tie-rod. In addition, the bottom track suffered local buckling along its flange. Fig. 10 presents the aforementioned damage as observed in Specimen SWWS-1 at a drift ratio of 4.12%.

Fig. 11 provides a comparison of the tension tie-rod forces for walls with and without a window opening with increasing normalized lateral force and drift. These plots demonstrate that the tension tie-rod force among window-no-window pairs is nominally unaffected, irrespective of whether the wall had a window opening. Comparison of wall end uplift and panel shear distortion evolution of the shear segment with increase in lateral force and lateral drift were also unaffected by presence of window opening.

Effect of Asymmetric Shear Wall

Two wall configurations included shear wall segments laid out in an asymmetric fashion. These walls had a 1.22-m long shear segment in-line with a 3.66-m long gravity bay. As a result, a direct comparison between walls with asymmetrical or symmetrical shear wall locations was possible. Fig. 12 shows the force-displacement response comparison between wall Specimens SGGS-1F and SGGG-1F, and Table 4 summarizes key response measurements. Results show that the asymmetric specimen reported lower lateral strength compared with the symmetrical specimen. Fig. 12 also shows the backbone comparisons of the two pairs of asymmetrical and symmetrical wall configurations (total of four specimen backbone curves).

After removing the additive effect of finishes, the asymmetric walls demonstrated 54% of the lateral strength of the symmetrical walls. Although the asymmetric walls had 50% of the shear segments compared with symmetrical walls, the 4% extra strength over the 50% may be anticipated due to be the contribution of the additional 1.22-m gravity segment. In addition, the elastic stiffness decreased by 53% for SGGG-1 compared with SGGS-1, and drift at strength was also lower for the asymmetric specimens. For the asymmetric specimen tested in the shake table test phase, SGGG-1, the accumulation of damage through the earthquake test sequence led to an elongation of the fundamental period from 0.233 s in its undamaged state to 0.348 s following the design-level earthquake test, compared with the symmetric Specimen SGGS-1 for which period elongation ranged from 0.157 to 0.199 s. Similarly, the damping ratio for SGGG-1 increased from 2.6% in its undamaged state to 11.4% after design-level earthquake test compared with SGGS-1 for which the damping ratio changed from 2.1% to 5.3%. Further discussion on evolution of dynamic characteristics for specimens tested during the shake table test phase has been given by Singh et al. (2020b).

Downloaded from ascelibrary.org by University of California, San Diego on 09/25/22. Copyright ASCE. For personal use only; all rights reserved.

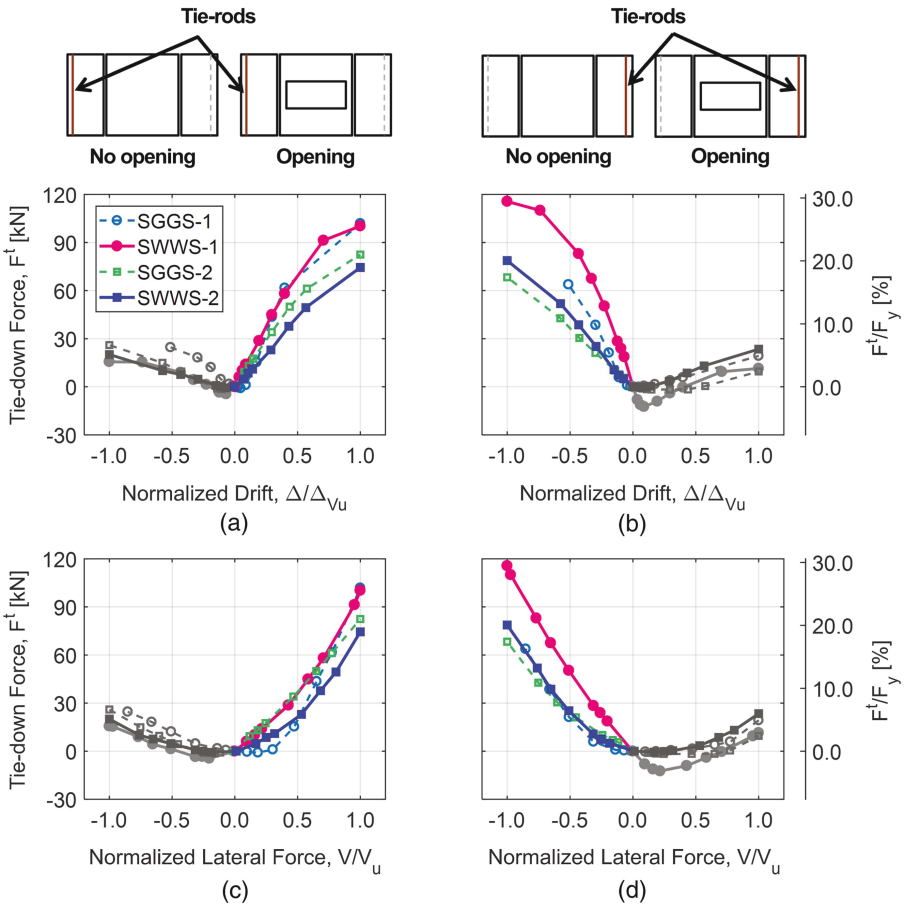

Fig. 11. Effect of window opening on tension-rod forces with increase in (a and b) normalized drift; and (c and d) normalized lateral force.

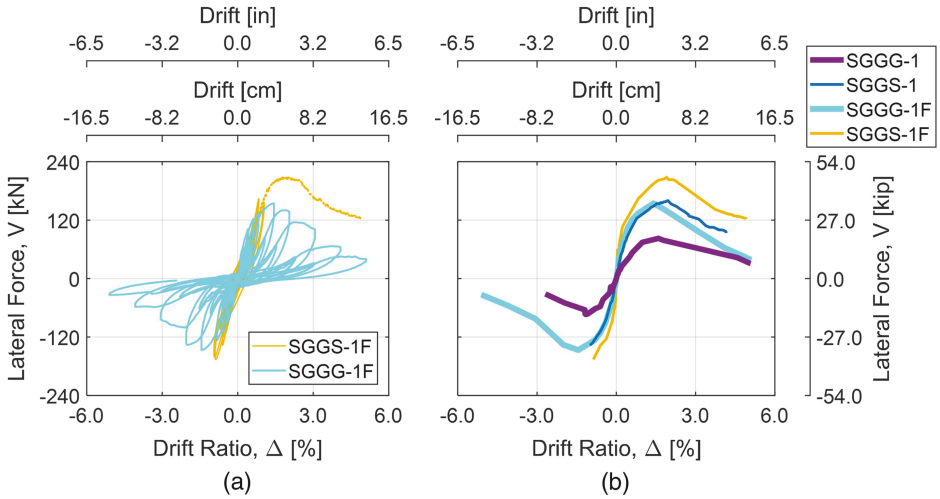

Fig. 12. Effect of asymmetric shear wall location: (a) force-displacement response; and (b) backbone curve comparison.

Asymmetric walls demonstrated a failure mode similar to their symmetrical counterparts. However, the failure, and any damage to framing members, were observed at lower drift ratio values for the asymmetric walls. Fig. 13 shows the damage observed in Specimen SGGG-1 following the final event in the dynamic testing sequence, during which it was pushed to a maximum drift ratio of 5.0%. During the low-intensity events, transient elastic sheet buckling was observed developing within a diagonal tension field as repeated cycles of relatively low drift demand were imposed. As drift demand increased to 1%, the width of the tension field and buckling of the steel sheet became more distributed, with lines of plastic deformation remaining prominently visible following a test.

Fastener tilting and bearing onto the steel sheet was visible in 20% of screws at test end for Specimen SGGG-1. Most of these were edge screws clustered at corners of sheet and midheight of field studs, which fell directly along the main diagonal of tension

Downloaded from ascelibrary.org by University of California, San Diego on 09/25/22. Copyright ASCE. For personal use only; all rights reserved.

Table 4. Effect of unsymmetrical shear wall location: results summary

Test phase	Specimen	Wall strength, V_u (kN)	Drift ratio at $0.4V_u$ (prepeak), $\Delta_{0.4Vu}$ (%)	Drift ratio at V_u (peak), Δ_{Vu} (%)	Drift ratio at $0.8V_u$ (postpeak), $\Delta_{0.8Vu}$ (%)	Elastic stiffness, K (kN/cm)
Shake table	SGGS-1	160.2	0.28	1.95	2.79	84.5
		—	−0.29	—	—	81.5
	SGGG-1	82.7	0.32	1.60	2.76	37.1
		−72.3	−0.26	−1.08	−1.53	41.0
	SGGS-1F	208.2	0.15	1.90	3.14	205.9
		—	−0.13	—	—	237.1
Quasi-static	SGGG-1F	156.8	0.17	1.41	2.35	74.7
		−144.5	−0.23	−1.43	−2.36	53.1

Note: 1 kN = 0.225 kip; and 1 kN/cm = 0.57 kip/in.

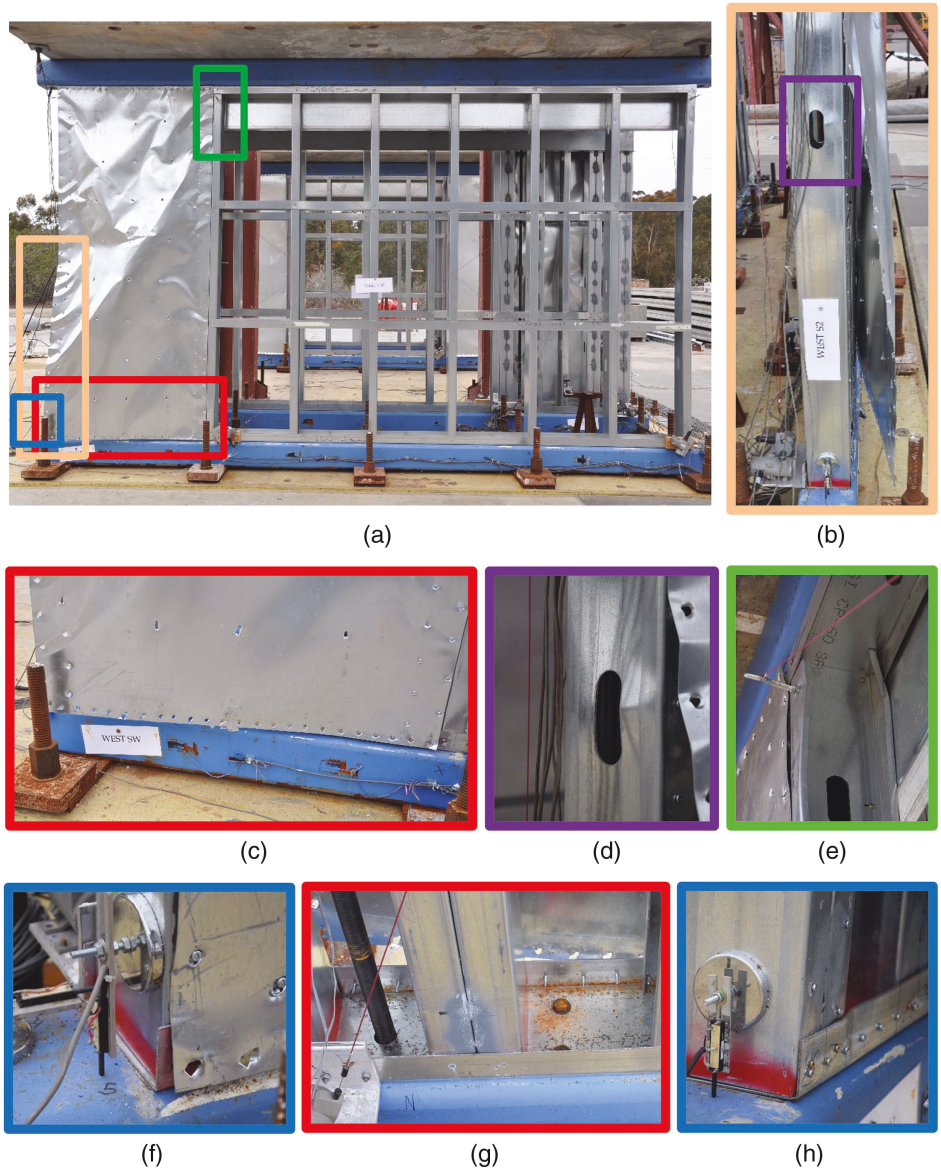

Fig. 13. (a–h) Pysical damage to Specimen SGGG-1 following the dynamic testing sequence, $\Delta_{max} = 5.1\%$ and $\Delta_{res} = 0.26\%$.

field. At the end of the dynamic testing sequence, the steel sheet had pulled over 40% of the fastener heads. The remaining screws also showed tearing or bearing due to tilting at a significant angle. The framing suffered extensive damage, including gravity studs adjacent to the shear segment and bottom track, which suffered local buckling. The chord stud packs and field stud framing connections suffered head shear failure, which caused the chord stud packs to slip along the bottom track.

Downloaded from ascelibrary.org by University of California, San Diego on 09/25/22. Copyright ASCE. For personal use only; all rights reserved.

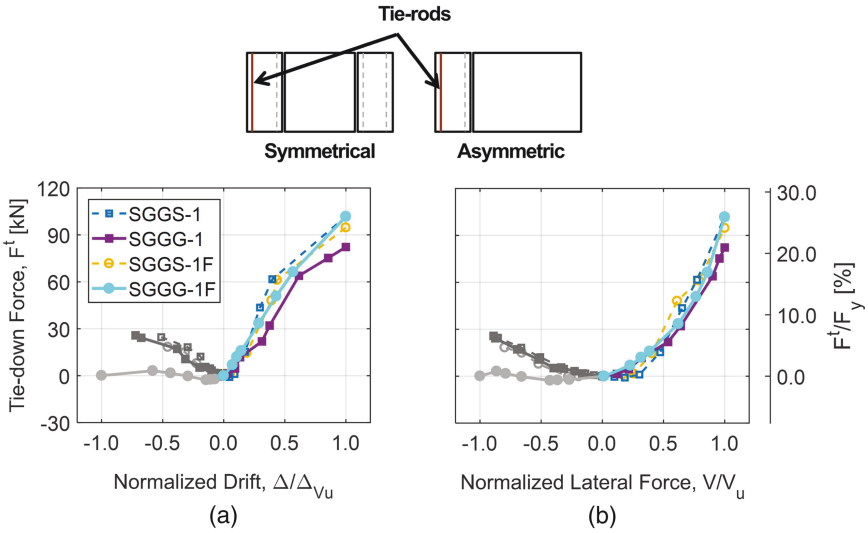

Fig. 14. Effect of asymmetric shear wall location on tension-rod forces with increase in (a) normalized drift; and (b) normalized lateral force.

Fig. 14 shows a comparison of the tension tie-rod force for the two pairs of asymmetrical and symmetrical wall specimens with increasing normalized lateral force and drift. At similar lateral force, the tension rods in the asymmetrical walls were subjected to larger axial forces compared with their symmetrical counterparts. However, when normalized by the individual specimen strengths, the tension rod forces were similar for the two pairs. Tension tie-rod force evolution was also similar for the two pairs when normalized for lateral drift. Due to their increased stiffness, the symmetrical walls experienced larger lateral force compared with the asymmetrical walls at similar lateral drift amplitudes, which resulted in larger axial forces in the tension tie-rods. Consistent with tension tie-rod forces, normalizing for individual specimen strengths or drift at strength, the evolution of wall uplift and panel shear distortion for the two pairs is quite similar. Figures showing the evolution of wall uplift and panel shear distortion with increase in lateral force and drift are not shown here for brevity.

Hysteretic Energy Dissipation

Because the specimens in the quasi-static test phase were subjected to the same loading protocol, the energy dissipation can be readily cross-compared at the different performance levels. Performance levels of interest are those defined for the shake table test phase, namely elastic, quasi-elastic, design, and above-design levels. These performance levels were defined according to the normalized lateral force and drift response of the individual specimens (Singh et al. 2021b). Dissipated energy is calculated as the area enclosed within the hysteresis of the force-displacement response and plotted against the cumulative drift of the specimen (Singh and Hutchinson 2022). Fig. 15(a) shows the comparison of cumulative energy dissipation with respect to cumulative drift ratio, $\Sigma\Delta$, normalized by the average cumulative drift ratio at strength in the two directions, $\Sigma\Delta_{Vu}$, for select specimens from the quasi-static test phase. These results are further synthesized by performance level and aggregated based on their common specimen variable in Fig. 15(b).

These figures show that wall configurations with finish application were consistently capable of dissipating about two to three times more energy compared with their unfinished counterparts. Only at larger drift cycles ($\Delta > 3.2\%$) did the dissipated energy from finished specimens become similar to that of their like unfinished specimens. This is indicated by the traces becoming parallel at larger cumulative drift ratios for finished and unfinished pairs. Such observations are consistent with the physical damage observed during testing, namely gypsum panels and the EIFS layer detached from the underlying wall framing at large drift amplitudes.

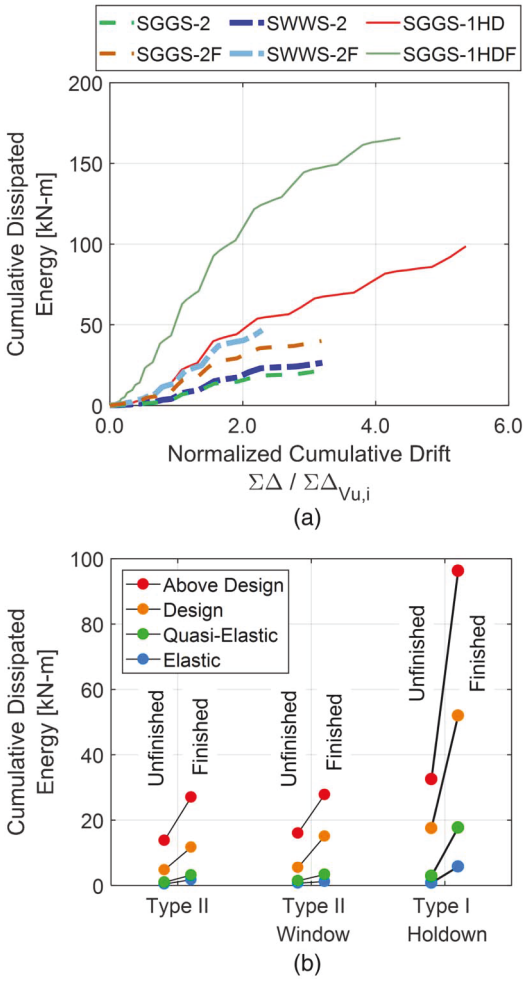

Fig. 15. (a and b) Cumulative dissipated energy comparison for select specimens from quasi-static test phase.

Downloaded from ascelibrary.org by University of California, San Diego on 09/25/22. Copyright ASCE. For personal use only; all rights reserved.

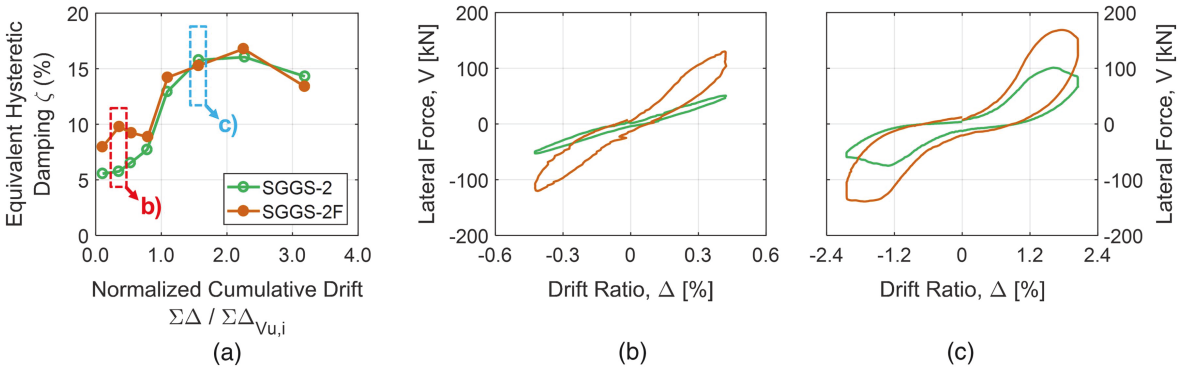

Fig. 16. Comparison of (a) equivalent hysteretic damping; and (b and c) hysteretic loops at elastic and above-design performance levels between SGGS-2 and SGGS-2F wall configurations.

The equivalent hysteretic damping, ζ, can also be computed on a per cycle basis using the global hysteretic response, as shown in Eq. (2)

$$\zeta = \frac{A_{\text{loop}}}{2\pi F_{\max} D_{\max}} \tag{2}$$

where A_{loop} = energy dissipated within a cycle in the hysteretic response; and $F_{\max}$ and $D_{\max}$ = maximum absolute force and the maximum absolute displacement in the cycle, respectively. Fig. 16 shows the comparison of equivalent hysteretic damping, ζ, with respect to cumulative drift ratio normalized by the average cumulative drift ratio at strength in the two directions for the Type II specimen pair SGGS-2 and SGGS-2F.

It can be observed from this figure that the equivalent hysteretic damping was larger for finished specimens at lower drift cycles and up to strength. Beyond strength, the equivalent hysteretic damping was similar for the two specimens. This same behavior was also observed for a Type II with window opening wall pair and a Type I with hold-downs wall specimen pair. A comparison of the hysteretic loops at elastic and above design performance levels is also shown in Figs. 16(b and c), respectively. These isolated full cycles articulate that the pinched behavior of the loops, and not the dissipated energy, governs the relative difference between the finished and unfinished configurations.

Conclusions

A two-phased experimental program examined 16 unique in-line wall configurations with several test variables with the goal of advancing the understanding of CFS-framed steel sheet sheathed shear wall-line behavior. The impact of variables governing the nonstructural detailing of CFS-framed walls, namely: finish application, window opening, and asymmetric shear wall location are discussed in this paper. The most prominent conclusions are as follows:

1. Finish application:
   - Finishes on a wall-line assembly substantially increased the wall strength without changing the wall failure mode. The additional strength from finish application has been quantified as 9.3 kN/m (635 lb/ft) for an exterior EIFS layer and 5.4 kN/m (370 lb/ft) for an interior gypsum panel layer. This increase was found to be independent of the underlying wall framing details.
   - The current design code AISI S400 (AISI 2015b) does not take into account the effect finish application has on wall behavior, particularly the increase in lateral-load capacity. It is recommended that overstrength due to finish be considered during the capacity design of tie-down components of CFS-framed systems.
   - The elastic stiffness also increased between 1.5 and 3 times when walls were finished on both faces. However, the drift at strength and the drift at 80% postpeak strength were not affected by the application of finishes.
   - The energy dissipated by the wall-line specimens was two to three times higher for finished configurations compared with unfinished configurations across the various target performance levels. The equivalent hysteretic damping was also larger for finished specimens up to strength, beyond which the effect of finishes was negligible.
2. Window opening:
   - Window openings detailed per design codes AISI S240 (AISI 2015a) and AISI S100 (AISI 2016) did not significantly effect wall seismic performance. Wall lateral strength and elastic stiffness as well as drift at strength for specimens with window opening were within 10% of that for configurations with similar framing but absent a window opening.
   - Nonetheless, the force transfer around the window opening resulted in larger stresses on adjacent chord stud packs. This led to failure of framing connection screws and slipping of stud packs, which is a cause for concern for maintaining structural integrity. This detailing issue needs further attention.
3. Asymmetric shear wall location:
   - Wall strength and stiffness were anticipated to reduce by 50% due to the explicit use of half the amount of shear walls in the asymmetric specimens. Measurements of both strength and stiffness were nominally consistent with this anticipated reduction.
   - Asymmetric walls demonstrated similar a failure mode as symmetrical walls. However, failure and damage to framing members were observed at lower drift ratios for asymmetric walls due to the overload imposed on a single shear wall segment within a wall line.

Results from this test program enrich the experimental database with documentation regarding the performance of CFS-framed wall assemblies by quantifying the impact of structural and nonstructural detailing variations commonly required in practice. The companion paper (Singh et al. 2022b) explains the experimental program and provides insight into the impact of structural detailing, and the present paper explored the impact of nonstructural detailing

Downloaded from ascelibrary.org by University of California, San Diego on 09/25/22. Copyright ASCE. For personal use only; all rights reserved.

such as architectural finishes and window openings on steel sheet sheathed CFS wall-lines. These research outcomes add valuable information to the ongoing development of seismic systems for buildings framed from CFS.

Data Availability Statement

The specimens tested under the CFS-NHERI experimental program were monitored with many analog sensors in addition to digital still cameras, several video cameras, and Global Positioning System (GPS) and unmanned aerial vehicles (UAVs) monitoring systems. High-quality data generated during the study are publicly available within the DesignSafe-CI repository (Singh et al. 2021a, 2022a).

Acknowledgments

The research presented herein is funded through the National Science Foundation (NSF) Grant Nos. CMMI 1663569 and CMMI 1663348, project entitled *Collaborative Research: Seismic Resiliency of Repetitively Framed Mid-Rise Cold-Formed Steel Buildings*. Ongoing research is a result of collaboration between three academic institutions: University of California, San Diego, Johns Hopkins University and University of Massachusetts, Amherst, two institutional granting agencies: American Iron and Steel Institute and Steel Framing Industry Association, and 10 industry partners. Industry sponsors include ClarkDietrich Building Systems, California Expanded Metal Products Co. (CEMCO), SWS Panel, SureBoard, United States Gypsum Corporation (USG), MiTek, Nevell Group, Atlas Tube, the Steel Network (TSN), and NBM Technologies; who each provided financial, technical, construction, and materials support. Specific individuals that dedicated significant time on behalf of this effort included Greg Ralph (ClarkDietrich), Fernando Sesma (CEMCO), Diego Rivera (SWS Panels), Tyler Elliot (SureBoard), Shahab Torabian (NBM Technologies), Esmaeel Rahmani and Jesse Karnes (MiTek), and Mike Korthals and Mark Wilson (Nevell Group). Regarding support for the test programs, the efforts of NHERI@University of California, San Diego, and Powell Labs staff, namely Noah Aldrich, Robert Beckley, Jeremy Fitcher, Abdullah Hamid, Dr. Christopher Latham, Darren McKay, Andrew Sander, Michael Sanders, and Alex Sherman, graduate students Filippo Sirotti and Maryam Soltani (University of Bologna, Italy), and several undergraduate students are greatly appreciated. Findings, opinions, and conclusions are those of the authors and do not necessarily reflect those of the sponsoring organizations.

Notation

The following symbols are used in this paper:

A_{loop} = energy dissipated within cycle (kN-m);
D_{max} = maximum absolute displacement in cycle (cm);
F^t = transient tie-down axial force (kN);
F_{max} = maximum absolute force in cycle (kN);
F_y = tension tie-rod measured yield point (kN);
K = elastic stiffness (kN/cm);
$K_{finished}$ = elastic stiffness of a finished specimen (kN/cm);
$K_{unfinished}$ = elastic stiffness of an unfinished specimen (kN/cm);
L = length of wall (m);
M_w = moment magnitude;
V = lateral force (kN);
V_{target} = percentage of wall strength (%);
V_u = wall strength (kN);
$V_{u,finished}$ = wall strength of a finished specimen (kN);
$V_{u,unfinished}$ = wall strength of an unfinished specimen (kN);
γ = shear distortion (%);
Δ = drift ratio (%);
Δ_{max} = maximum drift ratio (%);
Δ_{res} = residual drift ratio (%);
Δ_{target} = percentage of drift ratio at strength (%);
Δ_{Vu} = drift ratio at strength (%);
$\Delta_{Vu,finished}$ = drift ratio at strength of a finished specimen (%);
$\Delta_{Vu,unfinished}$ = drift ratio at strength of an unfinished specimen (%);
$\Delta_{0.4Vu}$ = drift ratio at 40% strength (prepeak) (%);
$\Delta_{0.8Vu}$ = drift ratio at 80% strength (postpeak) (%);
$\Delta_{0.8Vu,finished}$ = drift ratio at 80% strength (postpeak) of a finished specimen (%);
$\Delta_{0.8Vu,unfinished}$ = drift ratio at 80% strength (postpeak) of an unfinished specimen (%);
Δv_{EIFS} = strength increase due to EIFS layer per unit length (kN/m);
Δv_{gypsum} = strength increase due to gypsum panels per unit length (kN/m);
Δ^{γ} = contribution of shear distortion toward lateral drift (cm);
ζ = equivalent hysteretic damping (%);
$\Sigma\Delta$ = cumulative drift ratio (%);
$\Sigma\Delta_{Vu}$ = average cumulative drift ratio at strength in two directions (%); and
ϕ = rod diameter (mm).

References

AISI (American Iron and Steel Institute). 2015a. *North American standard for cold-formed steel structural framing*. AISI S240-15. Washington, DC: AISI.

AISI (American Iron and Steel Institute). 2015b. *North American standard for seismic design of cold-formed steel structural systems*. AISI S400-15. Washington, DC: AISI.

AISI (American Iron and Steel Institute). 2016. *North American specification for the design of cold-formed steel structural members*. AISI S100-16. Washington, DC: AISI.

ASCE/SEI (Structural Engineering Institute). 2017. *Seismic evaluation and retrofit of existing buildings*. ASCE/SEI 41-17. Reston, VA: ASCE/SEI.

Balh, N., J. DaBreo, C. Ong-Tone, K. El-Saloussy, C. Yu, and C. Rogers. 2014. "Design of steel sheathed cold-formed steel framed shear walls." *Thin-Walled Struct.* 75 (Feb): 76–86. https://doi.org/10.1016/j.tws.2013.10.023.

DaBreo, J., N. Balh, C. Ong-Tone, and C. Rogers. 2014. "Steel sheathed cold-formed steel framed shear walls subjected to lateral and gravity loading." *Thin-Walled Struct.* 74 (Jan): 232–245. https://doi.org/10.1016/j.tws.2013.10.006.

Filiatrault, A., D. Fischer, B. Folz, and C.-M. Uang. 2002. "Seismic testing of two-story woodframe house: Influence of wall finish materials." *ASCE J. Struct. Eng.* 128 (10): 1337–1345. https://doi.org/10.1061/(ASCE)0733-9445(2002)128:10(1337).

Krawinkler, H., F. Parisi, L. Ibarra, A. Ayoub, and R. Medina. 2001. *Development of a testing protocol for woodframe structures. CUREE Publication No. W-02*. Richmond, CA: Consortium of Universities for Research in Earthquake Engineering.

Liu, P., K. Peterman, and B. Schafer. 2014. "Impact of construction details on OSB-sheathed cold-formed steel framed shear walls." *J. Constr. Steel Res.* 101 (Oct): 114–123. https://doi.org/10.1016/j.jcsr.2014.05.003.

Lu, S. 2015. "Influence of gypsum panels on the response of cold-formed steel framed shear walls." Master's thesis, Dept. of Civil Engineering and Applied Mechanics, McGill Univ.

Downloaded from ascelibrary.org by University of California, San Diego on 09/25/22. Copyright ASCE. For personal use only; all rights reserved.

Morello, D. 2009. "Seismic performance of multi-storey structures with cold-formed steel wood sheathed shear walls." Master's thesis, Dept. of Civil Engineering and Applied Mechanics, McGill Univ.

Morgan, K., M. Sorhouet, and R. Serrette. 2002. *Performance of CFS framed shear walls—Alternative configurations*. Research Rep. No. LGSRG-06-02. Santa Clara, CA: Santa Clara Univ.

Nguyen, H., G. Hall, and R. Serrette. 1996. *Shear wall values for light weight steel framing*. Research Rep. No. LGSRG-3-96. Santa Clara, CA: Dept. of Civil Engineering, Santa Clara Univ.

Ong-Tone, C. 2009. "Tests and evaluation of cold-formed steel frame/steel sheathed shear walls." Master's thesis, Dept. of Civil Engineering and Applied Mechanics, McGill Univ.

Peterman, K., M. Stehman, R. Madsen, S. Buonopane, N. Nakata, and B. Schafer. 2016. "Experimental seismic response of a full-scale cold-formed steel-framed building. I: System-level response." *ASCE J. Struct. Eng.* 142 (12): 04016127. https://doi.org/10.1061/(ASCE)ST.1943-541X.0001577.

Salenikovich, A. J., D. J. Dolan, and S. W. Easterling. 2000. "Racking performance of long steel-frame shear walls." In *Proc., 15th Int. Specialty Conf. on Cold-Formed Steel Structures*. Rolla, MI: Univ. of Missouri–Rolla.

Schafer, B., Z. Zhang, and F. Haghpanah. 2020. "Overstrength in seismic design of cold-formed steel framed shear walls." In *Proc., Cold-Formed Steel Research Consortium Colloquium*. Baltimore: Cold-Formed Steel Research Consortium.

Schafer, B. W. 2011. "Cold-formed steel structures around the world: A review of recent advances in applications, analysis and design." *Steel Constr.* 4 (3): 141–149. https://doi.org/10.1002/stco.201110019.

Shamim, I., J. DaBreo, and C. A. Rogers. 2013. "Dynamic testing of single- and double-story steel-sheathed cold-formed steel-framed shear walls." *ASCE J. Struct. Eng.* 139 (5): 807–817. https://doi.org/10.1061/(ASCE)ST.1943-541X.0000594.

Singh, A., T. Hutchinson, X. Wang, Z. Zhang, B. Schafer, F. Derveni, H. Castaneda, and K. Peterman. 2021a. "Wall line tests: Phase 1—Shake table tests." In *CFS-NHERI: Seismic resiliency of repetitively framed mid-rise cold-formed steel buildings, DesignSafe-CI*. Salem, OR: NHERI. https://doi.org/10.17603/ds2-mvj8-8386.

Singh, A., T. Hutchinson, X. Wang, Z. Zhang, B. Schafer, F. Derveni, H. Castaneda, and K. Peterman. 2022a. "Wall line tests: Phase 2—Quasi-static tests." In *CFS-NHERI: Seismic resiliency of repetitively framed mid-rise cold-formed steel buildings, DesignSafe-CI*. Salem, OR: NHERI. https://doi.org/10.17603/ds2-encf-vj32.

Singh, A., and T. C. Hutchinson. 2022. "Lateral response of cold-formed steel framed steel sheathed in-line wall systems detailed for mid-rise buildings. Part II: Quasi-static test phase." In *Structural systems research project*. Rep. No. SSRP-19/06. La Jolla, CA: Univ. of California, San Diego.

Singh, A., X. Wang, and T. C. Hutchinson. 2021b. "Lateral response of cold-formed steel framed steel sheathed in-line wall systems detailed for mid-rise buildings. Part I: Shake table test phase." In *Structural systems research project.* Rep. No. SSRP-19/05. La Jolla, CA: Univ. of California, San Diego.

Singh, A., X. Wang, S. Torabian, T. C. Hutchinson, K. D. Peterman, and B. W. Schafer. 2020a. "Seismic performance of symmetric unfinished CFS in-line wall systems." In *ASCE structures congress 2020*, 629–642. Reston, VA: ASCE.

Singh, A., X. Wang, Z. Zhang, F. Derveni, H. Castaneda, K. Peterman, B. Schafer, and T. Hutchinson. 2020b. "Lateral response of cold-formed steel framed steel sheathed in-line wall systems detailed for mid-rise buildings." In *Proc., Cold-Formed Steel Research Consortium Colloquium*. Baltimore: Cold-Formed Steel Research Consortium.

Singh, A., X. Wang, Z. Zhang, F. Derveni, H. Castaneda, K. D. Peterman, B. W. Schafer, and T. C. Hutchinson. 2022b. "Steel sheet sheathed cold-formed steel framed in-line wall systems. I: Impact of structural detailing." *ASCE J. Struct. Eng.* 148 (12): 04022193. https://doi.org/10.1061/(ASCE)ST.1943-541X.0003433.

Steel Framing Alliance. 1997. *Monotonic tests of cold-formed steel shear walls with openings*. Research Rep. RP97-1. Washington, DC: American Iron and Steel Institute.

Uang, C.-M., and K. Gatto. 2003. "Effects of finish materials and dynamic loading on the cyclic response of woodframe shearwalls." *ASCE J. Struct. Eng.* 129 (10): 1394–1402. https://doi.org/10.1061/(ASCE)0733-9445(2003)129:10(1394).

Van Den Einde, L., et al. 2004. "Development of the George E. Brown Jr. network for earthquake engineering simulation (NEES) large high performance outdoor shake table at the University of California, San Diego." In *Proc., 13th World Conf. on Earthquake Engineering (WCEE)*. Vancouver, BC, Canada: WCEE Secretariat.

Yu, C. 2010. "Shear resistance of cold-formed steel framed shear walls with 0.686 mm, 0.762 mm, and 0.838 mm steel sheet sheathing." *Eng. Struct.* 32 (6): 1522–1529. https://doi.org/10.1016/j.engstruct.2010.01.029.

Yu, C., H. Vora, T. Dainard, J. Tucker, and P. Veetvkuri. 2007. *Steel sheet sheathing options for CFS framed shear wall assemblies providing shear resistance*. Rep. No. UNT-G76234. Denton, TX: Univ. of North Texas.

Downloaded from ascelibrary.org by University of California, San Diego on 09/25/22. Copyright ASCE. For personal use only; all rights reserved.